Developing high-performance reflective coatings for the tunable filter and the high-order interferometer of the 3D-NTT

Marie-Maude de Denus-Baillargeon[ab], Laëtitia Abel-Tibérini[b], Michel Lequime[b], Claude Carignan[acd], Benoît Épinat[d], Jean-Luc Gach[d], Olivier Hernandez[a], Michel Marcelin[d]

[a]Laboratoire d'Astrophysique Expérimentale, Université de Montréal, C.P. 6128 succ. Centre-Ville, H3C 3J7, Montréal (Qc), Canada ;
[b]Institut Fresnel, Domaine Universitaire St-Jérôme ave. Escadrille-Normandie, 13397 Marseille cedex 20, France ;
[c]Observatoire d'Astrophysique de l'Université de Ouagadougou, BP 7021, Ouagadougou 03, Burkina Faso ;
[d]Laboratoire d'Astrophysique de Marseille, Observatoire astronomique de Marseille-Provence, Technopôle de Château-Gombert, 38 rue Frédéric Joliot-Curie, 13388 Marseille, France ;

ABSTRACT

The following article describes the coatings of both Fabry-Perot (FP) etalons to be installed in the integral field spectrometer 3D-NTT. This simultaneous use of two FP etalons of high and low resolution respectively is the new concept upon which the 3D-NTT is built. Design and fabrication of the coatings of those etalons is a critical step to be able to achieve the desired performances of the instrument. More precisely, these etalons will have to show less than a 10% variation of the finesse from 370 to 900nm and a better than lambda/100 cumulative optical uniformity over a ⌀100mm surface. The aim is thus to design high-reflectivity coatings for each of the FP etalon. The design process of the two sets of coatings will be described first, then the expected performances of each etalon will be presented and finally the progresses in the making of these coatings will be discussed.

Keywords: Thin films optical coatings, Fabry-Perot interferometry, integral field spectro-imager, tunable filter

1. INTRODUCTION

The spectro-imager 3D-NTT is a new visiting instrument to be put in at the Nasmyth focus of the New Technology Telescope in 2009.Its distinctive feature is to use both high and low resolution FP etalons for observations in two different modes. The first is a tunable filter (TF) mode using only the low-resolution (LR) device at either the focus or the pupil plane. The second is a combined mode using both etalons simultaneously, the high resolution (HR) etalon working as a classical FP interferometer and the low resolution one acting as a selective filter to limit the number of order-blocking filters needed. In this last configuration, the low resolution and high resolution FP stand in the focus plane and the pupil plane respectively. To have a more general view of this instrument and its possibilities, please refer to the article from Marcelin et al.[1] to appear in this conference proceedings. The production of this instrument is already well under way, fruit of a collaboration between LAE (Laboratoire d'Astrophysique expérimentale, Canada), GEPI (OBSPM, France) and LAM (Laboratoire d'Astrophysique de Marseille, France).

To benefit fully from the versatility offered by two different modes of observation, each of the FP etalons had to show the following characteristics : (a) a working wavelength range extending from 370 to 850nm and (b) a possible resolution for every wavelength going from 100 to 30000 either in TF or combined mode.

Send correspondence to M.-M. de Denus.-Baillargeon. : E-mail : mmaude@astro.umontreal.ca

Since those FP etalons are part of a more complex system, certain constraints were already present and had to be taken into account when designing the coatings and simulating the performances : (a)NTT has a focal ratio of f/11 (b) the plates are ⌀120mm, 25mm-thick Corning HPFS fused-silica polished to $\lambda/1000$ rms and to $\lambda/100$ peak-to-valley over a ⌀100mm surface (c) the total displacement range of the actuators controlling the gap between the plates is $\Delta d = 200\mu m$.

The following section will describe the computer-aided design process and the results relative to the coatings themselves : reflectivity (%R), absorptivity (%A),phase at reflection (ϕ_R), number of layers and thicknesses. Then, from these characteristics of the individual plates, section 3 will make an overview of the expected performances in terms of order, finesse, and transmission characteristics of each of the FP etalon as an assembly, mentionning the tradeoffs on initial requirements to end up with productable versions of the coatings. Finally, section 4 will comment the control and fabrication process.

2. DESIGN

The reader will recall the following useful relations between the physical parameters of a FP etalon and the corresponding filtering characteristics of the system[2] :

$$\mathcal{R} = p\mathcal{F} \tag{1}$$

where $\mathcal{R} = \frac{\lambda}{\Delta\lambda}$ is the spectral resolution, p is the order of interference and $\mathcal{F}$ is the finesse of the etalon,

$$\mathcal{F} = \frac{\pi\sqrt{R}}{1 - R} \tag{2}$$

where R is the reflectivity of each plate of an etalon, and

$$p = \frac{2 \cdot n \cdot d}{\lambda} \tag{3}$$

where d is the physical gap between the plates, λ is the wavelength at which we evaluate the order and n is the refractive index of the spacer between the plates.

Then, it is also possible from those last parameters to calculate the free spectral range (FSR) and the full width at half max (FWHM) of each transmission peak of the Airy function :

$$\text{FSR} = \Delta\lambda = \frac{\lambda}{p} = \frac{\lambda^2}{2 \cdot n \cdot d}, \tag{4}$$

$$\text{FWHM} = \delta\lambda = \frac{\Delta\lambda}{\mathcal{F}}, \tag{5}$$

and from the transmissivity, reflectivity and absorptivity of each plate, the transmissivity of each Airy peak (T_{FP}) and the out-of-band extinction ratio (ρ_{FP}) :

$$T_{\text{FP}} = \frac{T^2}{(T + A)^2} \tag{6}$$

$$\rho_{\text{FP}} = 1 + \frac{4R}{(T + A)^2} \tag{7}$$

As one can see, the resolution for any given wavelength is theoretically completely defined by only two physical parameters : the reflectivity of each plate and the spacing between them. Equation 3 implies that the order varies with wavelength for a fixed spacing and thus the resolution as well. To get round this problem, two options present themselves : one can either make the reflectivity of the plates vary with wavelength as $\mathcal{F}(\lambda) \propto \lambda$, or design the FP assembly so the gap between the plates can be varied sufficiently to cover all the resolutions wanted at

TAB. 1. Physical and spectral characteristics of the FP etalons

	Low resolution	High resolution
Finesse	10	50
Reflectivity	$70.7 \leq \%R \leq 75.2$	$93.3 \leq \%R \leq 94.4$
Orders@600nm (TF)	9(17)- 676	—
Phys. Gap (TF)	2.5-202.5μm	—
Resolutions@600nm (TF)	90(170)-6760	—
Orders@600nm (comb.)	9(17)-115	120-1146
Phys. Gap (comb.)	2.5-34.5μm	143.9-343.9μm
Resolutions@600nm (comb.)	90(170)-1150	6000-57300

every wavelength. In our case, the latter solution has been selected for two principal reasons : $\mathcal{F}(\lambda) \propto \lambda$ entails a reflectivity pattern more complex to obtain than $R(\lambda) \propto cte$ and a constant finesse ensures a constant ratio between the free spectral range and full width at half max of the transmission peaks.

The piezoelectric actuators included in the assembly of the etalons have a displacement range of 200μm, with a lowest spacing of 2.5μm. The lower spacing conditions the finesse wanted for the low order etalon (for a minimal resolution of 100). As for the high resolution etalon, the requirement was a finesse of 50. It was decided that the finesse should not vary by more than 10% over a range of a FSR for the lowest orders used for every etalon.

For a summary of the characteristics of each etalon, see table 1. Design of the thin films stacks for each etalon was done with computational help through the optimization softwares OptiLayer[3] and OpenFilters.[4] The design method with these softwares follow this general scheme, based on a trial-and-error approach for the initial design aspect :

1. choose the materials and substrate to use

2. define the reflectivity targets for the spectral characteristics of the coating for the whole wavelength range

3. input a starting design

4. optimize with one of the available methods

5. clean the design of all physically un-depositable layers

6. go through the steps 2 to 5 of the process again, changing either the starting design or the targets if the design did not evolve to an appropriate solution

7. when the design is found satisfactory, %R, %T, %A and ϕ_R of the obtained mirrors are computed.

The design softwares offer a variety of optimization methods, but only two were used in the present study : the refinement method and the needles method. The first method is simply an optimization of the merit function of the stack with regard to the target when each layer's thickness is varied, while the second method is based on the introduction in a given layer of an infinitesimally-thin layer of the different index material at the most favorable point. This second method is always followed by another iteration of the first method to let the needle "grow" to its optimal thickness.

Two different types of design were explored : all-dielectric designs and metal-dielectric designs. For higher reflectivities, all-metal or metal-dielectric solutions are unsuitable since the thicknesses of metallic layers needed to cause such %R values will also bring about absorptivity high enough to "kill" the transmission peak (see eq. 6). To keep a T_{FP} value of more than 90%, the absorptivity of each mirror must not be higher than 1.45% and 0.33% for the LR and HR coatings respectively. Thus, only all-dielectric stacks were investigated for the HR coatings. SiO_2, Ta_2O_5 and HfO_2 are available as dielectric materials and Ag as a metal. The dielectric materials present good optical and mechanical properties (appropriate indexes, low absorption, dense films, unaffected by humidity) and Ag, albeit more fragile to scratches, stays stable over time. Their optical characteristics are summarized in table 2. The data for dielectric materials come from experimental analysis of deposited layers and the values for silver come from Johnson and Christy.[5] The reflecting band of an all-dielectric stack has a spectral

TAB. 2. Optical characteristics of the chosen materials

Material	n@600nm	k@600nm
Ta_2O_5	2.12	$< 10^{-3}(t.b.d.)$
HfO_2	2.03	$< 10^{-3}(t.b.d.)$
SiO_2	1.47	$< 10^{-4}$
Ag	0.06	4.005

width of

$$\Delta\left(\frac{\lambda_0}{\lambda}\right) = \frac{2}{\pi}\sin^{-1}\left(\frac{n_H - n_L}{n_H + n_L}\right) \tag{8}$$

where λ_0 is the design wavelength, n_H and n_L are the refractive indexes of the high and low n materials respectively.[6] This relation infers a net advantage to take materials with highly different refractive index. Likely, a high index shock will lead to more reflective coatings for the same number of layers. To achieve reflectivity on a large wavelength range, the usual technique is to stack reflectors designed at different wavelengths. These basic reflectors are achieved by stacking one high and one low index layer over the substrate (HL). Stacking several of these reflectors (HLHLHL) causes the reflectivity of the mirror to increase. The typical design will then be[7] :

$$a(HL)^A b(HL)^B ...(HL)^C ...d(HL)^D e(HL)^E, \tag{9}$$

where H and L represent layers which optical thicknesses are $\lambda/4$ of the considered wavelength for high and low index materials respectively. $A, B, C, ...$ is the number of repetitions of the basic reflective stack (HL), and $a, b, c, ...$ is a coefficient multiplying the thickness of the individual layers (that allows to fix a different center wavelength for each reflector to be stacked). As an example, $1.2(HL)^2 0.9(HL)$ would correspond to 1.2H 1.2L 1.2H 1.2L 0.9H 0.9L. For practical feasability reason, the total physical thickness of the coatings had to be limited. Correspondingly, the maximum number of layers for the high and low resolution designs were 45 and 25. Initial designs were typically limited to 2/3 of this number to be able to use efficiently the needles method.

Needles and refinement methods are sensitive to local minima in the merit function of the stack. Therefore, several trials were made using sligthly different values of the $a, b, c, ...$ and $A, B, C, ...$ coefficients to control the overlap of the different reflection bands. For the metal/dielectric designs, the starting design was : $(HL)^2 A$, where A is a layer of silver of 10nm thick. A few layers of low thicknesses is the most general design for computational optimization techniques.[8]

Figures 1 and 2 show the caracteristics of the most satisfactory designs for both etalons. Because of the lower refractive index of HfO_2, designs with this material require a higher number of layers to obtain the same reflectivity performances. The high resolution coatings designs are made of 47 (Ta_2O_5/SiO_2, total thickness $3.9\mu m$) and 54 (HfO_2/SiO_2, total thickness $4.3\mu m$) layers respectively. As for the low resolution coatings, the number of layers are 19 (Ta_2O_5/SiO_2, total thickness $1.59\mu m$), 25 (HfO_2/SiO_2, total thickness $1.78\mu m$) for the all-dielectric designs and 9 ($Ta_2O_5/SiO_2/Ag$, total thickness 341nm) and 11 ($HfO_2/SiO_2/Ag$, total thickness 671nm) for metal-dielectric case.

The lower graphs of figure 2 show a net difference in the behavior of the phase at reflection (ϕ_R) of metal/dielectric and all-dielectric stacks : phase at reflection varies a lot faster with respect to the wavelength for the all-dielectric than for the metal/dielectric design. The main reason for that is the smaller number of layers needed in presence of a metallic layer to show the same overall reflectivity as the all-dielectric stack. The thicker the dielectric stack, the most rapidly admittance changes between two given wavelengths, which is also why the high resolution coating shows a very rapid variation of the phase with wavelength. The requirement for a continuous and $\simeq$ constant reflectivity over an extended spectrum increases the number of layers needed in the coatings and thus the variation of ϕ_R with λ. The effects of this phase at reflection is a well known problem[9] and will be discussed in the next section.

3. SIMULATED PERFORMANCES OF THE ASSEMBLY

In the present context, it is not so much the individual properties of each plate that are interesting but their performances as a Fabry-Perot assembly. As such, the important parameters discussed in this section are the
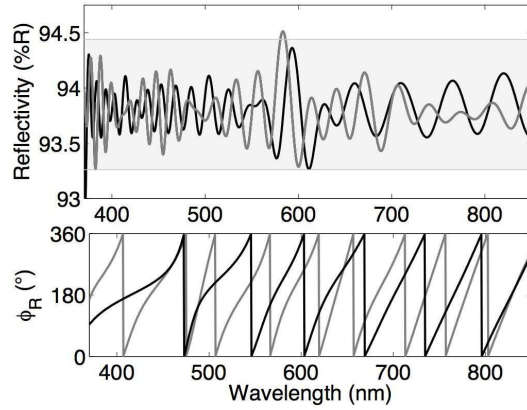
FIG. 1. Reflectivity and phase at reflection of the high resolution coatings design. The solid black and solid grey lines are the Ta_2O_5/SiO_2 and HfO_2/SiO_2 designs respectively. Reflectivity requirements are represented by the shaded area.
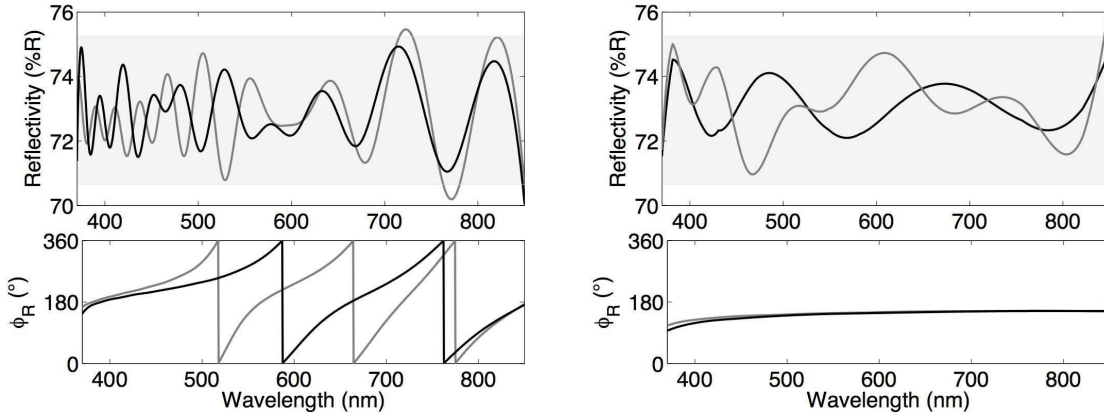
FIG. 2. Reflectivity and phase at reflection of the low resolution coatings design. On left panel the solid black and solid grey lines are the Ta_2O_5/SiO_2 and HfO_2/SiO_2 designs respectively, whereas in right panel the same line colors represent $Ta_2O_5/SiO_2/Ag$ and $HfO_2/SiO_2/Ag$. Reflectivity requirements are represented by the shaded area.

effective order and finesse, the transmissivity of the assembly, and the performances of the instrument with the simultaneous use of both etalons.

3.1 Performances of both etalons

The finesse of the etalon can be calculated directly from the reflectivity of the plates from eq. 2. For the effective order, in reality it is not as straigthforward as eq. 3 lets imagine. The transmitted intensity of a beam of light as a function of wavelength follows this equation :

$$I(\lambda) = I_0(\lambda) \cdot \frac{T(\lambda)^2}{(1 - R(\lambda))^2} \cdot \frac{1}{1 + \frac{4R(\lambda)}{(1-R(\lambda))^2} \sin^2(\phi_R(\lambda) - \frac{2nd}{\lambda})}, \tag{10}$$

where $\phi(\lambda)$ is the phase at reflection of each plate. It then follows that the wavelength of the transmission peaks are not only determined by the spacing between the plates but also from the phase at reflection of the coatings. Thus the deviation of the phase from a constant means that the peaks will be either more or less spaced than in the ideal case, and the effective order will no longer be defined by eq.3. This effective order is particularly important for the use of the low resolution FP since it lays down a lower limit on the resolution domain attainable in tunable filter mode. This arises from eq.1. The calculation of the effective order was here done numerically by

evaluating $I(\lambda)$ and finding the FSR at one specific wavelength. Figure 3 sums up the lowest achievable orders for the low resolution etalon.

As seen on fig. 3, the influence of ϕ_R on the effective order is obvious. For the metal/dielectric coatings, the
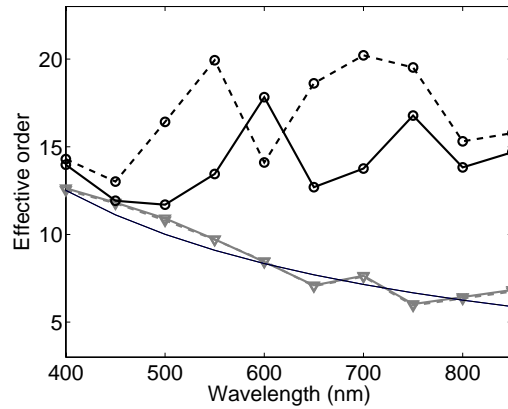
FIG. 3. Effective order of the low resolution coatings design with respect to the wavelength for a spacing $d = 2.5\mu$m. The gray set of lines (with "$\triangledown$") represents metal/dielectric designs : "—" $SiO_2/Ta_2O_5/Ag$ and "- -" $SiO_2/HfO_2/Ag$. The black set of lines (with "$\bigcirc$") represents all-dielectric designs :"—" SiO_2/Ta_2O_5 and "- -" SiO_2/HfO_2. The thin black solid line represents the order of an ideal FP.

effective order is very close to the ideal order whereas it deviates significantly for both all-dielectric designs, and further more where the slope of ϕ_R vs. λ is steepest. It is possible to control the phase dispersion over a small wavelength range[10, 11] but none of the trials of starting designs converged to a satisfying solution for such an extended wavelength range as the one needed here. The effective orders and resolutions attainable with this TF are given in table 1, where the number in parenthesis represents the case for which ϕ_R affects the most the lowest effective order. From this domain of resolution available in TF mode, the minimal spacing of the high resolution etalon was calculated for a continuous domain of resolutions.

On the question of order, the metal-dielectric design seems to be the best available option, but one has to take into account the absorptivity of such coatings, which proves to be a major obstacle to high throughput of the assembly. Figure 4 shows the effect of the current metal/dielectric designs on the transmissivity of the low resolution FP etalon at its lowest plate separation distance and emphasizes the unacceptable transmissivity for the shortest wavelengths.
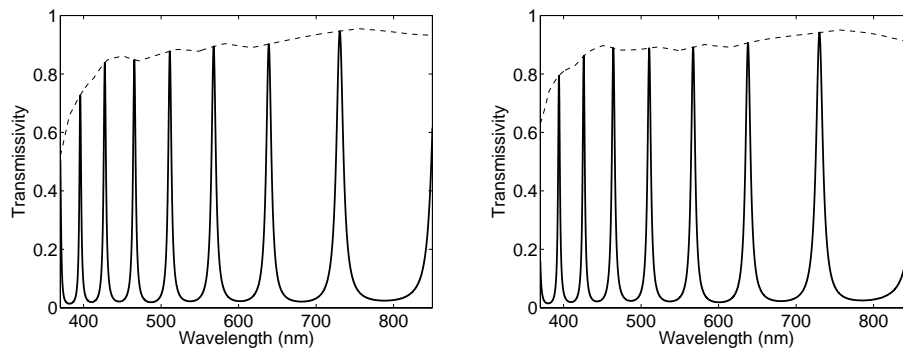
FIG. 4. **Left panel** : Transmissivity of a FP etalon of $SiO_2/Ta_2O_5/Ag$ design. **Rigth panel** : Transmissivity of a FP etalon of $SiO_2/HfO_2/Ag$ design. In both panels, the dotted line is the transmissivity enveloppe

The last element to be taken into account is the effect of the position of etalons in the optical path. Both

etalons will be used at the pupil plane; the low resolution when in TF mode, and the high resolution when in combined mode. This is the classical case of use of FP etalons. The low resolution etalon will also be used at the focal plane of the telescope when used in combination with the high resolution etalon, and in another case as a TF to avoid problems due to phase change throughout the field of view associated with the use at pupil plane. In the present case, the beam has a focal ratio of f/11 with a central obstruction (secondary mirror) of f/34. This, of course, leads to light coming from different parts of the mirror to be transmitted at different central wavelengths. This causes an effective broadening of the FWHM. Figure 5 shows the effect of the etalon being at focus plane for the lowest and highest available order. The widening of the FWHM becomes much of a problem when the etalon is used at an order of $\simeq 100$, where the elemental FWHM are very small comparing to their difference in central wavelength. This leads to the overall transmission peak to fall at very low throughput values (below $\simeq 80\%$) and will prevent the use of the LR etalon in TF mode at focus for resolutions ranging from ~ 1500 to 6000.
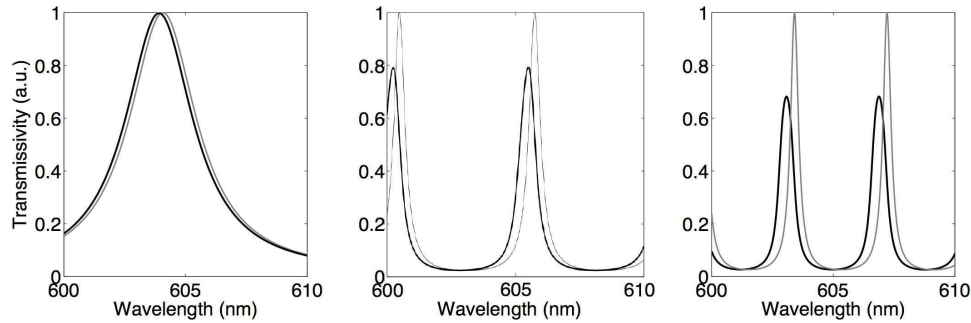
FIG. 5. Example of the effect of the focal ratio on the transmission characteristics of the LR etalon at different orders for a Ta_2O_5/SiO_2 coating. Left panel : order 14 (lowest possible order with a d=2.5μ) Middle panel : order 115 (highest order needed for combination mode). Right panel : order $\simeq 150$

Another problem arising from the use of the low resolution etalon at focus is the local variation of thickness induced by imperfections in the polish. Despite the very good quality (<3nm rms) of the plates, this small error becomes significant at focus : the gap between the plates is then changed and causes the transmitted wavelength to shift sligthly from place to place on the etalon. By defocusing the etalon by a few cm, the beam spot partly evens out this effect and reduces by a factor 2 the change in wavelength.

3.2 Cascading mode

The original aspect of the instrument 3D-NTT is the use of both etalons in combined mode. This section summarizes the general resulting spectral characteristics when both etalons are used in this manner.

For the low resolution FP to act as a useful order-selecting filter, ISLs and FWHMs of the two etalons must be well matched. A compromise has to be reached to keep the maximum transmission and still ensure an acceptable selectivity. This situation arises when $\text{FSR}_{HR} \leq \text{FWHM}_{LR}$ (see figure 6). With the help of equations 4 and 5 this condition can be expressed in either way :

$$R_{LR}\mathcal{F}_{HR} \leq R_{HR} \tag{11}$$

$$p_{LR}\mathcal{F}_{LR} \leq p_{HR} \tag{12}$$

From the resolution obtained at $d = 202.5\mu m$ for the LR etalon in TF mode, it is possible to deduce the minimal order to have a continuous range of resolutions and introduce a shim between the plates to control the minimal order of the high resolution etalon. This means orders ranging from 12 to 115 for the LR etalon and 120 to 1146 for the HR etalon in combination mode. When FSR_{HR} and FWHM_{LR} are not strictly equal, more than one transmission peak might be over the 50% threshold. This is not a problem since the observations are output as data cubes : every "slice" of the cube is an image of an object at a small different $\Delta\lambda$ or, considered the other way around, each pixel yields a spectrum. By looking at the spectrum, it is possible to see if two different peaks are exactly one FSR_{HR} appart. Except very peculiar cases, it is simply an order skip.
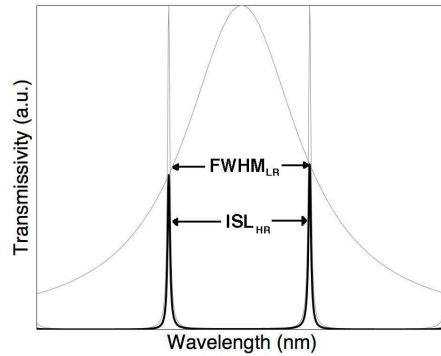
FIG. 6. Resulting spectral characteristic of the instrument in combination mode. Curves in grey are the individual transmission spectra of each etalon and the curve in black is the resulting spectrum when both are used in combination

4. FABRICATION PROCESSES

The coatings of these etalons will be processed in a Dual Ion Beam Sputtering (DIBS) and an Ion Assisted Deposition (IAD) deposition systems. Both systems provide dense and stable materials. DIBS combines two ion beams to achieve reactive sputtering. The first beam sputters a metal target and the second beam is used directly on the sample as an assistance for densification and chemical reaction completion. As for the IAD process, it is an evaporation system (the materials are heated and not sputtered) with an ion beam assistance directly on the sample. In both systems, HfO_2, Ta_2O_5 and SiO_2 are available materials and Ag is deposited in IAD only. Fabrication of such devices requires careful control of every step of the deposition process. Since a minimal error on certain layers can have dire consequences, the control is done by direct measurement of the optical properties *in situ* in real time. Both deposition system are equipped with a broadband optical monitoring system. A white light beam shines through the sample during deposition and the resulting spectrum is measured (see figure7). A
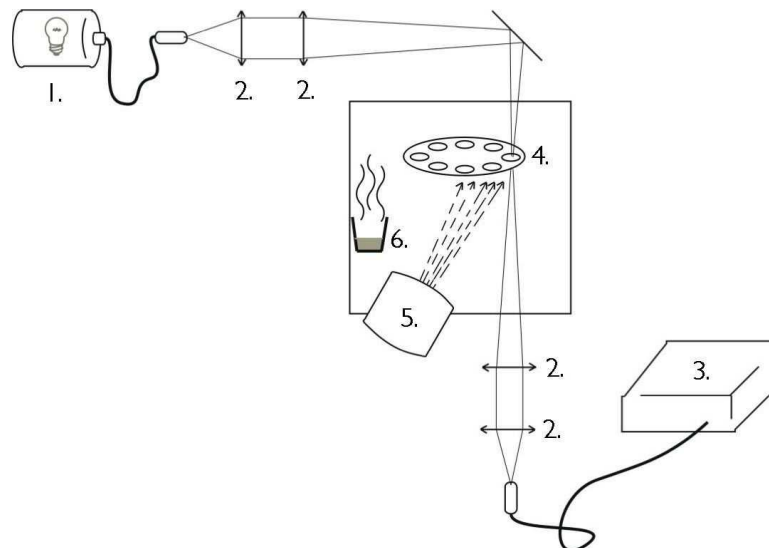
FIG. 7. Diagram of the IAD deposition system. 1—white light source (fiber output) 2—collimation lenses 3—spectrometer 4—substrate holder 5—ion source 6—precursor crucible

simulation of the expected spectra at each elemental increase of the thickness is stored in the control computer, allowing to know with a precision $\simeq 0.1$nm the thickness of the layer, provided the refractive index is known

for each control λ. The control software also has a re-optimization algorithm adjusting the remaining layers thicknesses to compensate for errors made previously.[12]

Errors on fabrication of less than 0.5nm 68% of the time and less than 1nm 97% of the time were reported with this setup of optical monitoring.Figure 8 show the effect of fabrication errors on the R and ϕ_R characteristics for all designs. As is possible to see on figure 8, no design has a big advantage over the other in terms of degradation
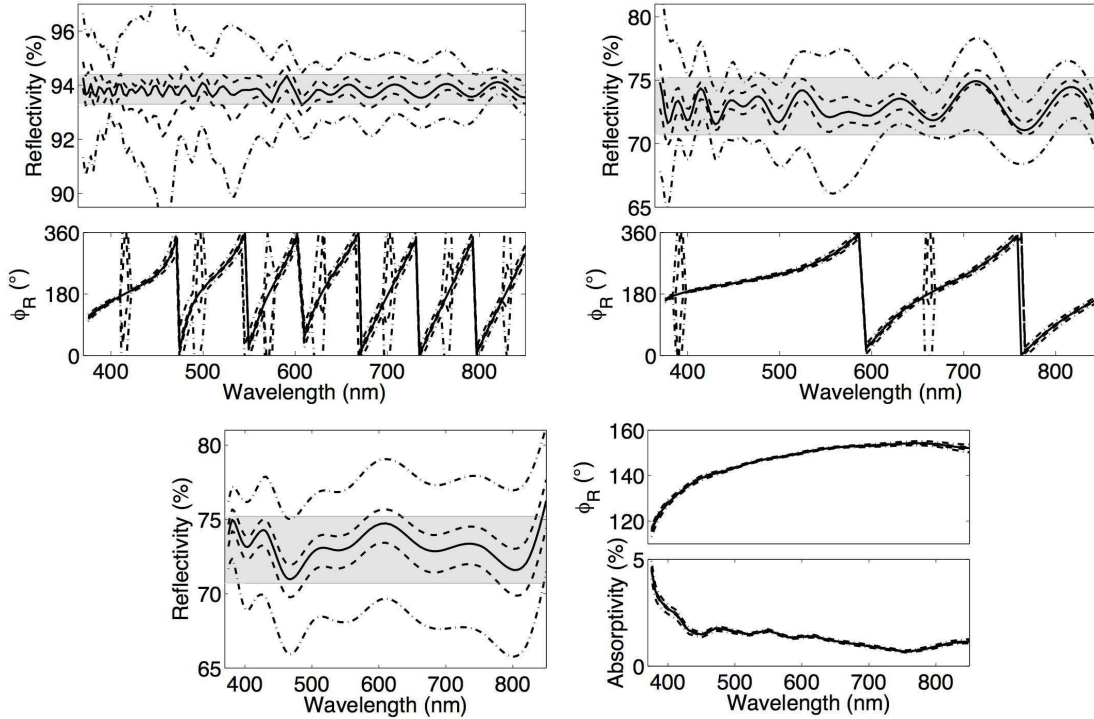
FIG. 8. Example of the probability domain of reflectivities of different designs with respective errors of "- -" 0.5nm and ".-" 1nm. Panel a) HR design (SiO$_2$/Ta$_2$O$_5$) b)LR all-dielectric design (SiO$_2$/Ta$_2$O$_5$) c)LR metal/dielectric design (SiO$_2$/HfO$_2$/Ag). Shaded area represents the required reflectivity boundaries.

of the reflectivity when errors are made upon fabrication. In all cases, errors beyond 0.5nm cause the plausible resulting curve to diverge significantly from the reflectivity boundaries set by the finesse requirements. In the case of the metal/dielectric designs, the effect on both phase and absorptivity is minimal.

5. CONCLUSIONS

As a highly versatile instrument, the spectro-imager 3D-NTT brings its share of challenges for the design of all constitutive components. The work presented here is the conception of a few different designs and study of the inferred properties of the resulting Fabry-Perot etalons. The initial requirements and related constraints were the following :
  – a wavelength range of 370-850nm ;
  – a finesse of 10 for the LR etalon and 50 for the HR etalon with a maximum variability of 10% over a FSR at lowest order ;
  – the lowest possible order for the LR etalon ;
  – more than 90% transmissivity for the assembled etalon ;
  – 200μm displacement range of the actuators controlling the gap ;
  – resolutions from 100 to 30000 for all wavelengths

Two different designs for the high resolution (SiO_2/Ta_2O_5, 47 layers, thck : $3.9\mu m$;SiO_2/HfO_2, 54 layers, thck : $4.3\mu m$) and four different designs for the low resolution (SiO_2/Ta_2O_5, 19 layers, thck : $1.6\mu m$; SiO_2/HfO_2, 25 layers, thck : $1.8\mu m$; $SiO_2/Ta_2O_5/Ag$, 9 layers, thck : 341nm, $SiO_2/HfO_2/Ag$, 11 layers, thck : 671nm) etalons were set with the help of informatics design tools. Designs including metals were ruled out because of their unacceptable absorptivity in the blue region of the spectrum, despite their net advantage on the topic of effective orders. Similarly, for fabrication reasons, the SiO_2/Ta_2O_5 designs are preferred because they are thinner and have a lesser number of layers. In all cases, statistical errors of up to 0.5 nm can be tolerated and still give finesse results inside requirement limits.

The resolutions covered by the system when in TF mode range from 140(170) to 1000 when the etalon is placed in the focal plane but goes up to 6760 when it is standing in the pupil plane. Limits for the focal plane are due to the angular spread of the beam causing a deformation of the transmission peak. For the combined mode, the resolutions range from 6000 to 57300.

These are theoretical resolutions for perfect coatings. We will also have to take into account production of a suitable anti-reflective coating on the backside of the plates, the effect of the stress of the stack and the uniformity of the coatings and what it implies as a degradation of performances for the Fabry-Perot assembly, all problems that will have to be assessed as the fabrication process goes on.

ACKNOWLEDGMENTS

REFERENCES

[1] Marcelin, M., Amram, P., Balard, P., Balkowski, C., Boissin, O., Boulesteix, J., Carignan, C., Daigle, O., de Denus-Baillargeon, M.-M., Épinat, B., Gach, J.-L., Hernandez, O., Rigaud, F., and Vallée, P., "3D-NTT : a versatile integral field spectro-imager for the NTT," in [*SPIE Conference Astronomical Telescope and Instrumentation, Marseille June 23-28, 2008.*], *Proc. SPIE*, t.b.d (2008).

[2] Born, M. and Wolf, E., [*Principle of optics :electromagnetic theory of propagation, interference and diffraction of light (6th ed.)*], Cambridge University Press, Cambridge, UK (1997).

[3] Tikhonravov, A., Trubetskov, M., and deBell, G., "Application of the needle optimization technique to the design of optical coatings," *Applied Optics* **35**, 5493–5508 (1996).

[4] Larouche, S. and Martinu, L., "Openfilters : open source software for the design, optimization and synthesis of optical filters," *Applied Optics* **47**, C219–C230 (2008).

[5] Johnson, P. and Christy, R., "Optical constants of the noble metals," *Physical Review B* **6**, 4370–4379 (1972).

[6] MacLeod, A., [*Thin-Films Optical Filters, 3rd edition*], Institute of physics publishing, London, UK (2001).

[7] Turner, A. and Baumeister, P., "Multilayers mirrors with high reflectance over an extended spectral region," *Applied Optics* **5**, 69–76 (1966).

[8] Baumeister, P., "Starting designs for the computer optimization of optical coatings," *Applied Optics* **34**, 4835–4843 (1995).

[9] Tikhonravov, A., Baumeister, P., and Popov, K., "Phase properties of multilayers," *Applied Optics* **36**, 4382–4392 (1997).

[10] Troitski, Y., "Synthesis of mirrors with anomalous dispersion of the reflection phase," *Optical Engineering* **34**, 1503–1507 (1995).

[11] Lemarquis, F. and Pelletier, E., "Optical coating without phase dispersion for a Fabry-Perot interferometer," *Applied Optics* **35**, 4987–4992 (1996).

[12] Badoil, B., *Contrôle spectrophotométrique large bande de filtres interférentiels en cours de dépôt*, PhD thesis, Université Paul-Cézanne Aix-Marseille III (2007).